

Existence of wormholes in the spherical stellar systems

A. Övgün* and M. Halilsoy†

*Physics Department, Eastern Mediterranean University,
Famagusta, Northern Cyprus, Mersin 10, Turkey.*

(Dated: June 2, 2022)

Potentiality of the presence of wormholes in the outer/inner regions of the halos of galaxies, situated on the Navarro-Frenk-White (NFW) density profile and Universal Rotation Curve (URC) dark matter models are investigated recently [1–3]. Since this covers our own galaxy also as a possible home for wormholes it prompts us to further the subject by considering alternative density distributions. From this token herein we make use of the Einasto model [4–6] to describe the density profiles for the same purpose. Our choice for the latter is based on the fact that theoretical dark matter halos produced in computer simulations are described best by such a profile. For technical reasons we trim the number of parameters in the Einasto profile to a possible minimum. Based on such a model it is shown that wormholes in the outer regions of spiral galaxies are possible while the central regions prohibit such formations.

PACS numbers:

Keywords: wormholes, Milky Way, spherical stellar systems, galaxies, halos, dark matter

I. INTRODUCTION

Recently, F. Rahaman et al. have used both the NFW [7]

$$\rho(r) = \frac{\rho_s}{\left(1 + \frac{r}{r_s}\right)^2}, \quad (1)$$

and URC dark matter density profiles [8]

$$\rho(r) = \frac{\rho_0 r_0^3}{(r + r_0)(r^2 + r_0^2)} \quad (2)$$

where ρ_0 , ρ_s , r_0 and r_s are all constants, to show the potentiality of the presence of wormholes in the outer and the place closer to central region, respectively, of the halo.

In this paper, following similar line of thought, we study the Einasto model [4–6] which is the special function that arrange the finest total fit to the halo density profiles. It tells how the density ρ of a spherical stellar system alter with distance r from its center [9]:

$$\rho(r) \approx e^{-Ar^\alpha} \quad (3)$$

with constants A and α .

The bounded parameter α adjusts the degree of curvature of the profile, given exactly by the function

$$\rho(r) = \rho_0 \exp \left[-\frac{2}{\alpha} \left(\left(\frac{r}{r_0} \right)^\alpha - 1 \right) \right]. \quad (4)$$

and is plotted in Fig. 1. For the Milky Way galaxy, we have $r_0 = 9.11$ kpc and $\rho_0 = 5 \times 10^{-24} (r_0/8.6 \text{ kpc})^{-1} \text{ gcm}^{-3}$.

The slopes of the NFW profile has the range from the inner/outer ($r \rightarrow 0$ / $r \rightarrow \infty$) are depicted in Figs 2, 3 and 4 below. On the other hand, the values are different for the Einasto profile which are included as limiting cases of isothermal and Gaussian, ($\alpha = 0$, $\alpha = 2$, respectively). The difference between the Einasto and NFW profiles

*Electronic address: ali.ovgun@emu.edu.tr

†Electronic address: mustafa.halilsoy@emu.edu.tr

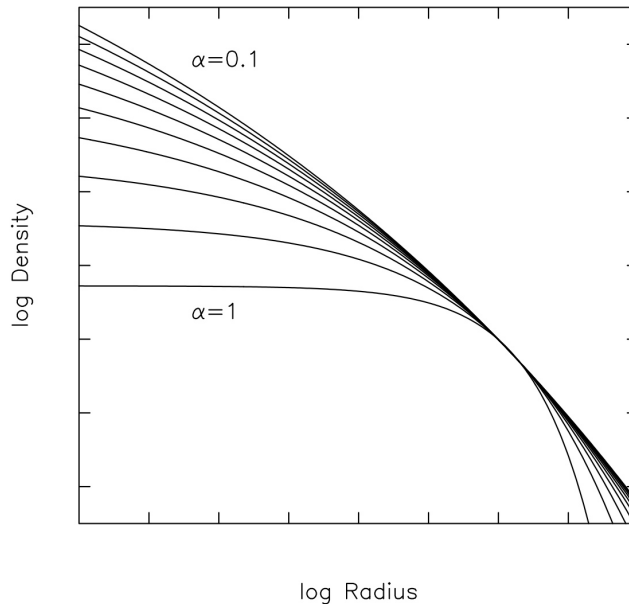


FIG. 1: Einasto profile in log-log plot (the parameter α controls the degree of curvature of the profile) from Eqn. 3 .

appears at small and large radial distances. After all, on scales of concern for gas or stellar dynamics and strong gravitational lensing the Einasto profile with $\alpha = 0.25$ is very akin to the NFW profile, and on scales of concern for weak gravitational lensing the Einasto profile with $\alpha = 0.2$ is rather significant to the NFW profile. Galaxy mass halos typically have $\alpha = 0.16$ as referred in Fig 2,3 and 4 [10].

Einasto's model has been used in the description of many systems, such as galaxies, and halos. It is used to show the dark matter profiles of simulated halos as well as the NFW profile [13–15]. The Einasto profile has a finite (zero) central slope, in contrast to the NFW profile which has a divergent (infinite) central density. Due to the restricted resolution of N-body simulations, it is unclear yet which model description fit well to the central densities of simulated dark-matter halo. The observations of both the Milky Way and some galaxies may be compatible with the NFW profile for the dark matter halo [12, 16–19]. The dark matter profile of smaller galaxies tend to have flatter distributions of dark matter in the central region, known as the cuspy halo problem[20, 21]. Our purpose in this paper is to search for possible wormholes in a spiral galaxy specified by the Einasto density profile. Wormholes are solutions to Einstein's equations that connect different universes or tunnels through different parts of the same universe. Our primary aim is to consider the Milky Way galaxy as a test bed for this venture. To this end we choose the parameter r_0 of Milky Way to coincide with the throat of the wormhole whereas the second parameter α is in a restricted range. From the Einstein equations we derive the equations for the density and pressures in terms of the metric functions and their derivatives. Although our analytical functions are expressed in terms of the Whittaker functions [22] the detailed analysis are not imperative. It suffices for us to check the null-energy condition and satisfaction of the flare-out conditions [23]. The same technical handicap prevents us to investigate the stability of the resulting wormhole that may exist in the Milky Way galaxy. It is observed that at the central region Einasto profile does not give a wormhole solution because violation of null energy condition is not satisfied there. But in the outward region we obtain possible wormholes.

The paper is organized as follows. In Sec. II we present the Einstein equations for wormhole space-time and we find their solutions under the Einasto dark matter profile. In Section III we discuss our results and conclude the paper.

II. WORMHOLES UNDER THE EINASTO DARK MATTER PROFILE

The spherically symmetric and static wormhole geometry which was proposed by Morris-Thorne is given by the line element [23]

$$ds^2 = -e^{2f(r)} dt^2 + \left(1 - \frac{b(r)}{r}\right)^{-1} dr^2 + r^2(d\theta^2 + \sin^2 \theta d\phi^2), \quad (5)$$

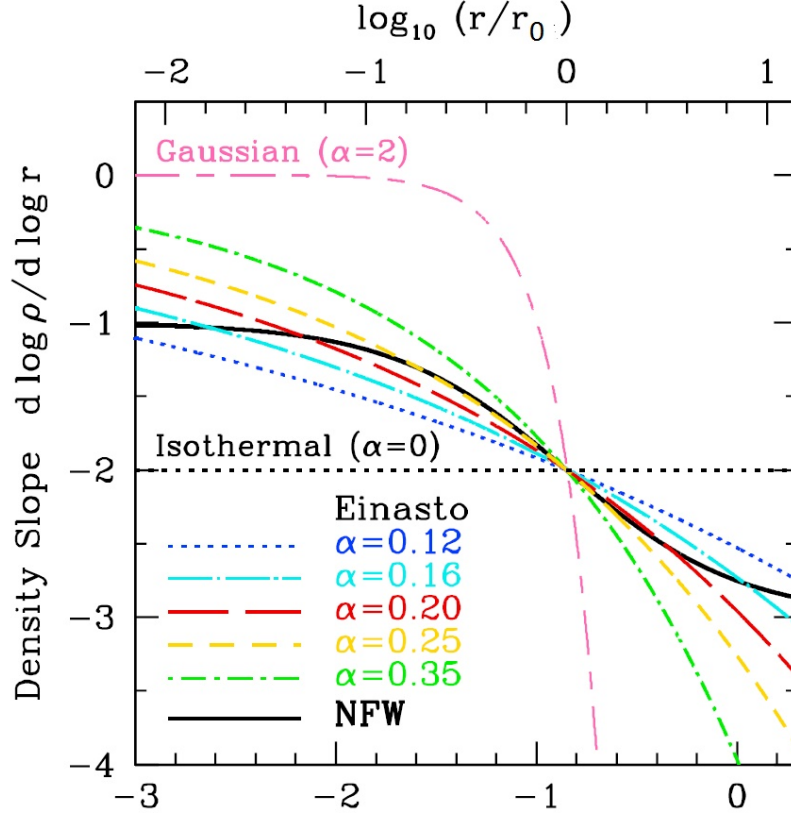


FIG. 2: Density profiles of Einasto and NFW, density slope ($d \log \rho / d \log r$), [10]

where the function $b(r)$ defines the spatial shape function, and $f(r)$ stands for the redshift function. The radial coordinate r ranges from $+\infty$ to $b(r_0) = r_0$ (minimum radius). The minimum value of the r is r_0 , called the throat of the wormhole. The proper radial distance is given by

$$l(r) = \pm \int_{r_0}^r \frac{dr}{\sqrt{1 - \frac{b(r)}{r}}}. \quad (6)$$

Properties of such wormholes are listed below [23];

- Spherically symmetric, static metric
- Satisfy the Einstein field equations
- No event horizon, i. e. $e^{f(r)} \neq 0$
- "Throat" $r = r_0$ connects two asymptotically flat space-time regions
- Reasonable stress-energy tensor (violating the null-energy condition (NEC) with $\rho + p_r < 0$, where ρ is the energy density and p_r the radial pressure)
- Satisfy the flare-out condition at the throat ($b'(r_{th}) < 1$, while $b(r) < r$ near the throat)
- Finite and reasonable crossing time
- Stable against perturbations

The Einstein field equation to be satisfied, is given by

$$G_{\mu\nu} = 8\pi T_{\mu\nu} \quad (7)$$

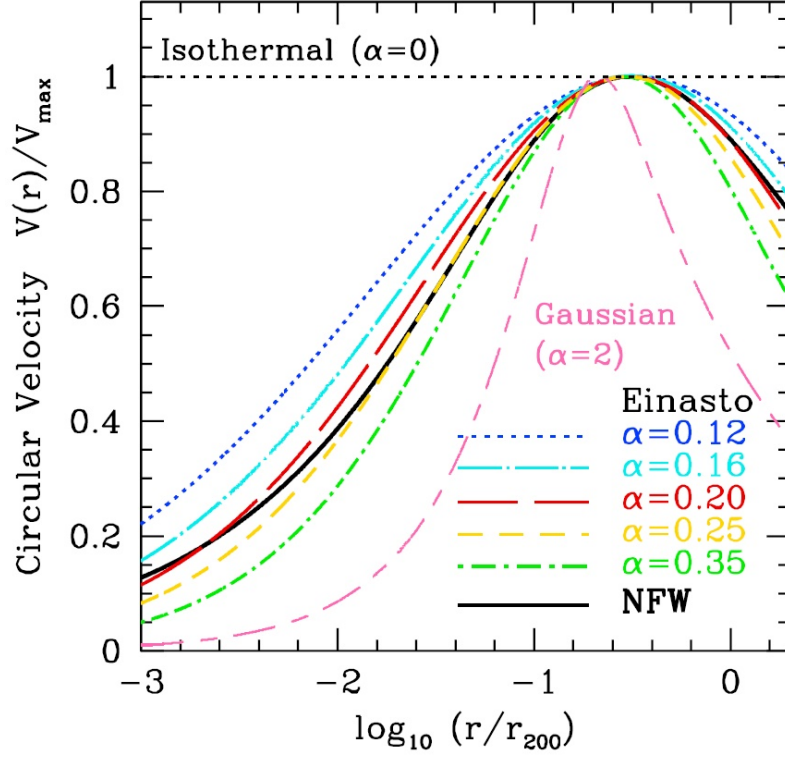


FIG. 3: Comparison of NFW (solid black lines) and Einasto (colored lines) profiles. In this example the halo concentration $c_{200} = 7.1$ [10]

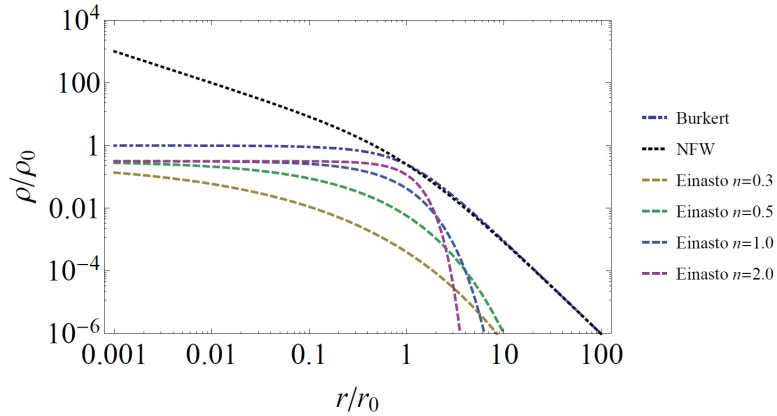


FIG. 4: Comparison of the density profiles for different phenomenological models of dark matter distribution [11]

where $T_{\mu\nu}$ is the stress-energy tensor, $G_{\mu\nu}$ is the Einstein tensor with the units in which $c = G = 1$. Field equations relate space-time curvature to matter and energy distribution as stated in Misner, Thorne, Wheeler (MTW) in their book "Gravitation" that "Space acts on matter, telling it how to move. In turn, matter reacts back on space, telling it how to curve". The non-zero $G_{\mu\nu}$ components are

$$G_{tt} = \frac{b'}{r^2}, \quad (8)$$

$$G_{rr} = \frac{-b}{r^3} + 2\left(1 - \frac{b}{r}\right)\frac{f'}{r}, \quad (9)$$

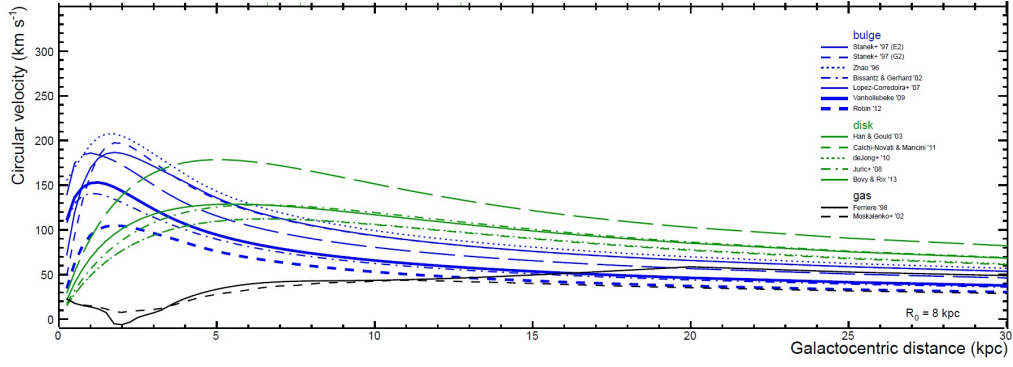


FIG. 5: Rotational velocity curve for Milkyway (the contribution to the rotation curve as predicted from different models for the stellar bulge (blue), stellar disk (green) and gas (black). We assume a distance to the galactic center $r_0 = 8$ kpc [12])

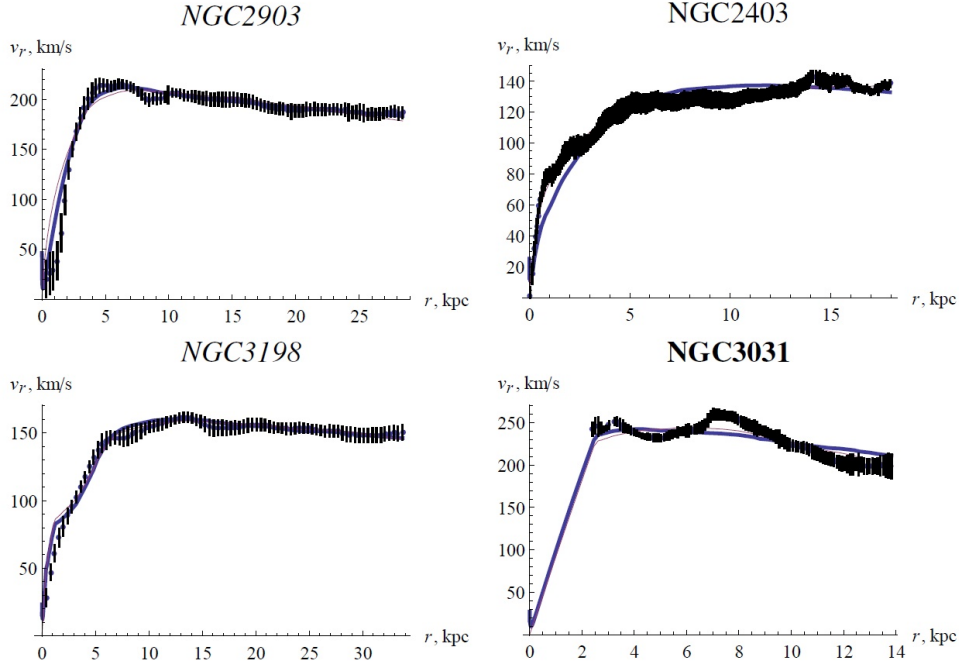


FIG. 6: Rotational curves $v(r)$ for some galaxies from THINGS survey together with fits. Blue thick curves show best fits by dark matter distributions of semi-degenerate configurations, while magenta thin curves show Einasto profile best fits [11]

$$G_{\theta\theta} = G_{\phi\phi} = \left(1 - \frac{b}{r}\right) \left[f'' + f'^2 + \frac{f'}{r} - \left(f' + \frac{1}{r}\right) \left\{ \frac{b'r - b}{2r(r-b)} \right\} \right], \quad (10)$$

in which a prime is $\frac{d}{dr}$.

It is assumed that dark matter is expressed in the form of general anisotropic energy-momentum tensor [24], as follows

$$T_{\nu}^{\mu} = (\rho + p_t)u^{\mu}u_{\nu} - p_t g_{\nu}^{\mu} + (p_r - p_t)\eta^{\mu}\eta_{\nu}, \quad (11)$$

in which $u^{\mu}u_{\mu} = -\eta^{\mu}\eta_{\mu} = -1$, and where p_t is the transverse pressure, p_r is the minimum pressure and ρ is the energy density. The only non-zero components of $T_{\mu\nu}$ are

$$T_{tt} = \rho, \quad (12)$$

$$T_{\theta\theta} = p_r, \quad (13)$$

$$T_{\phi\phi} = p_t. \quad (14)$$

Furthermore we need to impose some constraints in order to solve Einstein field equations. One of them is the tangential velocity [25, 26]

$$v^\phi = \sqrt{r f'} \quad (15)$$

which is responsible to fit the flat rotational curve for the dark matter. Other one is proposed by F. Rahaman et. al [2] that the observed rotational curve profile in the dark matter region is given by

$$v^\phi = \alpha r \exp(-k_1 r) + \beta [1 - \exp(-k_2 r)] \quad (16)$$

in which α , β , k_1 , and k_2 are constant positive parameters. It is illustrated in Fig.7. With this choice it is guaranteed that for $r \rightarrow \infty$ we obtain $v^\phi = \beta = \text{constant}$ which is required for flat rotation curves.

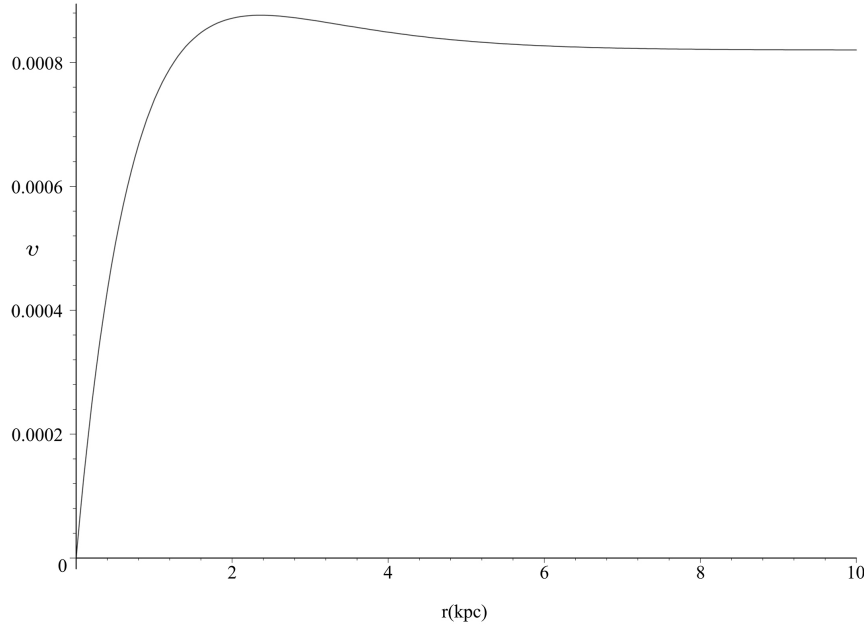


FIG. 7: Proposed rotational velocity with values of the parameters as $k_1 = k_2 = 1, \alpha = 0.0006$ and $\beta = 0.00082$ [2]

From the Eqns.(15) and (16), one obtains the redshift function as follows

$$f(r) = -\frac{\alpha^2 r}{2k_1 e^{(2k_1 r)}} - \frac{\alpha^2}{4k_1^2 e^{(2k_1 r)}} - \frac{2\alpha\beta}{k_1 e^{(k_1 r)}} + \frac{2\alpha\beta e^{(-k_1 r - k_2 r)}}{k_1 + k_2} + \beta^2 \ln(r) + 2\beta^2 E_i(1, k_2 r) - \beta^2 E_i(1, 2k_2 r) + D. \quad (17)$$

with the exponential integral E_i [27] and integration constant D . For large r , it is required also that $e^{2f(r)} = B_0 r^{(4v^\phi)}$ [28, 29].

By using the Eqns. (15) and (16) and the Einasto density profile (Eqn. (4)), the Einstein field equations give us the tedious form of the shape function

$$b(r) = \frac{2^{(3-\frac{3}{\alpha})} \pi \rho_0}{\alpha} \exp\left(\frac{2}{\alpha}\right) \left(\frac{(r/r_0)^\alpha r^{-\alpha}}{\alpha}\right)^{-3/\alpha} \left[\left(\frac{1}{3(\alpha+3)(2\alpha+3)}\right) \alpha^3 r^3 2^{(3/\alpha-1-(\alpha+3)/2\alpha)} \left(\frac{(r/r_0)^\alpha r^{-\alpha}}{\alpha}\right)^{3/\alpha} \right. \\ \left. \times (2(r/r_0)^\alpha + \alpha + 3)(r/r_0)^{-\alpha} \left(\frac{(r/r_0)^\alpha}{\alpha}\right)^{-(\alpha+3)/2\alpha} \right] \quad (18)$$

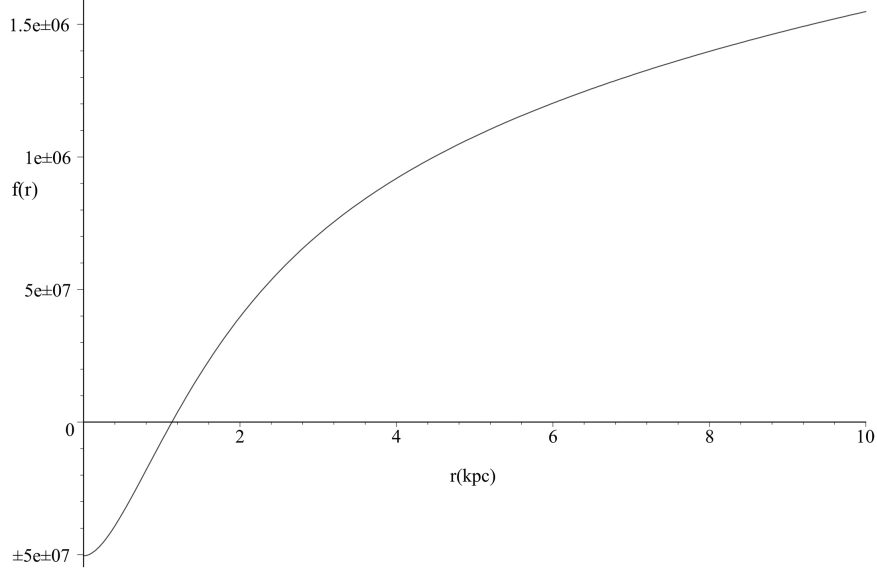


FIG. 8: $f(r)$ versus r ($k_1 = k_2 = 1, \alpha = 0.0006$ and $\beta = 0.00082$ [2])

$$\begin{aligned}
 & \times \exp\left(-\frac{(r/r_0)^\alpha}{\alpha}\right) WhittakerM(3/\alpha - (\alpha + 3)/2\alpha, (\alpha + 3)/2\alpha + 1/2, \frac{2(r/r_0)^\alpha}{\alpha}) \\
 & + \left(\frac{1}{3(2\alpha + 3)}\right) \alpha^2 r^3 2^{(3/\alpha - 1 - (\alpha + 3)/2\alpha)} \left(\frac{(r/r_0)^\alpha r^{-\alpha}}{\alpha}\right)^{3/\alpha} (\alpha + 3)(r/r_0)^{-\alpha} \\
 & \times \left(\frac{(r/r_0)^\alpha}{\alpha}\right)^{-(\alpha + 3)/2\alpha} \exp\left(-\frac{(r/r_0)^\alpha}{\alpha}\right) WhittakerM(3/\alpha - (\alpha + 3)/2\alpha + 1, (\alpha + 3)/2\alpha + 1/2, \frac{2(r/r_0)^\alpha}{\alpha})] + C_1
 \end{aligned}$$

where the integration constant is chosen as

$$C_1 = \frac{-r_0}{6\alpha^2 + 27\alpha + 27} \left(A\pi r_0^2 \exp(1/\alpha) 2^{(3\alpha - 3)/2\alpha} \alpha^{1 + (\alpha + 3)/2\alpha} \right) \quad (19)$$

$$\begin{aligned}
 & [\alpha(5 + \alpha) WhittakerM(-(\alpha + 3)/2\alpha, (2\alpha + 3)/2\alpha, 2/\alpha) \\
 & + (3 + \alpha) WhittakerM((\alpha + 3)/2\alpha, (2\alpha + 3)/2\alpha, 2/\alpha) - 6\alpha - 9].
 \end{aligned}$$

Note that in this expression WhittakerM stands for the Whittaker function [22]. The redshift function $f(r)$ versus radial coordinate r is plotted in Fig.8.

It can be checked that the wormhole throat condition of $b(r_0) = r_0$ is satisfied. It is shown in Figs 9 and 10. For the Milky Way galaxy, we have $r_0 = 9.11$ kpc and $\rho_0 = 5 \times 10^{-24} (r_0/8.6 \text{ kpc})^{-1} \text{ g cm}^{-3}$ [8, 30, 31]. Furthermore, the flare-out condition ($b' < 1$) is also satisfied for the Milky Way galaxy $b'(r_0) = 0.98 \times 10^{-20} < 1$ (Fig.11).and also all spherical stellar systems as shown in Fig. 12. In addition, both the star-count and kinematic data of the Milky Way stellar halo are well-represented by an Einasto profile with index $\alpha \approx 0.5$ and effective radius ≈ 20 kpc, if the dark halo has a flat rotation curve (Figs 4, 5 and 6) [32] .

The radial and lateral pressures are calculated implicitly as

$$p_r = \frac{1}{8\pi} \left(\frac{-b}{r^3} + 2\left(1 - \frac{b}{r}\right) \frac{f'}{r} \right), \quad (20)$$

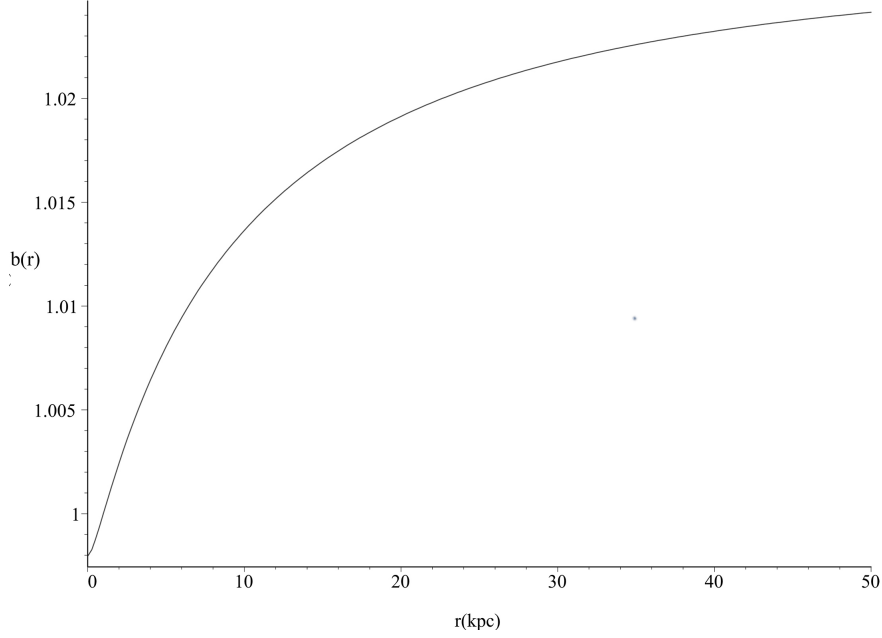


FIG. 9: The shape function b versus radial coordinate r with the parameters $r_0 = 1$ and $\rho_0 = 0.0001$

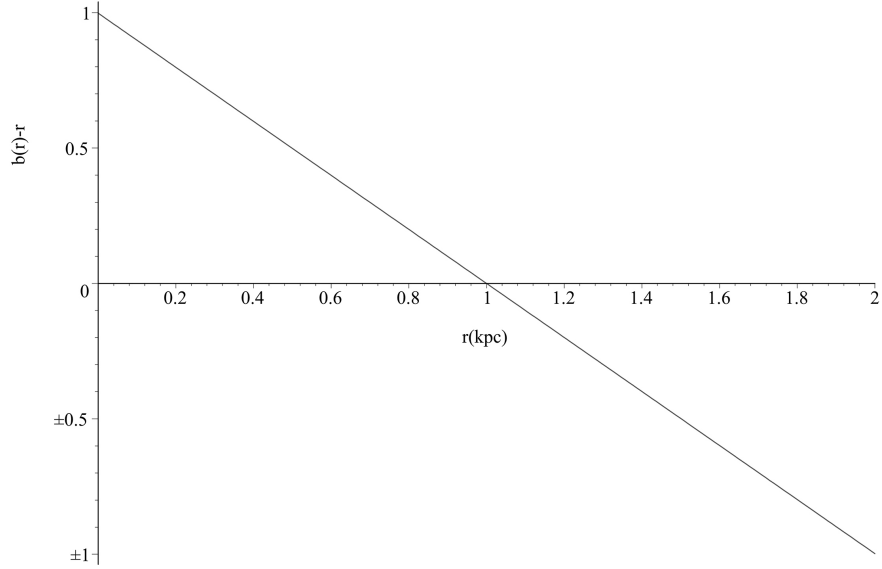


FIG. 10: The radius of the throat is obtained where $b(r)-r$ cuts r axis or the values $r_0 = 1$ and $\rho_0 = 0.0001$

$$p_t = \frac{1}{8\pi} \left\{ \left(1 - \frac{b}{r} \right) \left[f'' + f'^2 + \frac{f'}{r} - \left(f' + \frac{1}{r} \right) \left(\frac{b'r - b}{2r(r-b)} \right) \right] \right\} \quad (21)$$

in which $f(r)$ and $b(r)$ are to be substituted from the solution (Eqn.s 17- 19). For technical reasons this will not illuminate us much and therefore will be ignored.

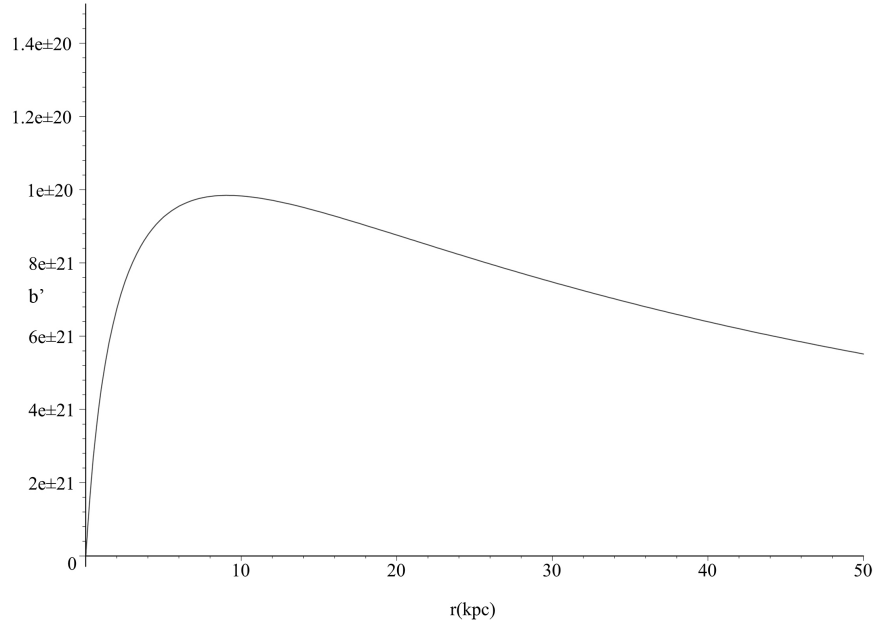


FIG. 11: b' versus r for Milky Way ($r_0 = 9.11$ kpc and $\rho_0 = 5 \times 10^{-24} (r_0/8.6 \text{ kpc})^{-1} \text{ g cm}^{-3}$ [8, 30, 31])

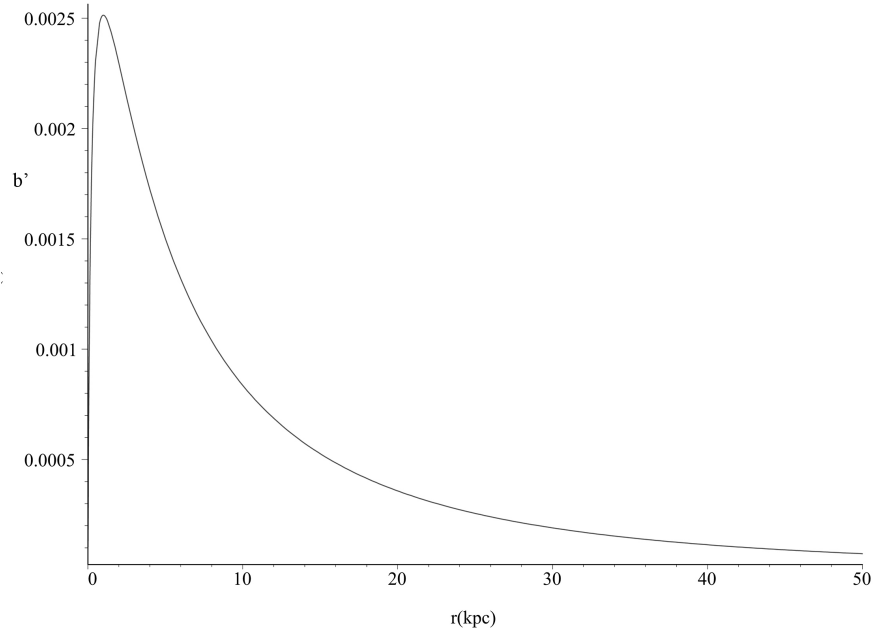


FIG. 12: b' versus r ($r_0 = 1$ and $\rho_0 = 0.0001$)

The null energy condition ($\rho + p_r < 0$) is also violated so flare-out condition for wormhole is satisfied according to Fig. 13.

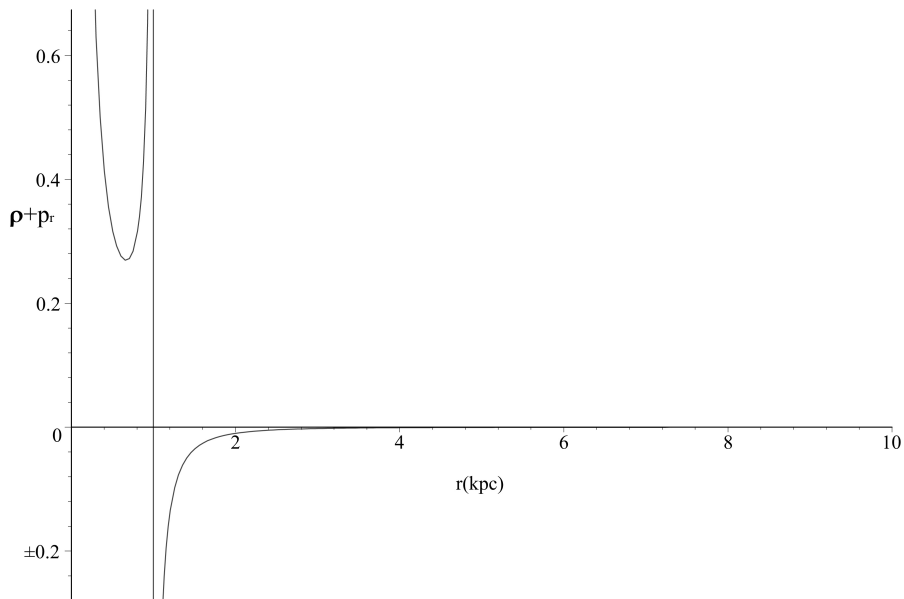


FIG. 13: Null energy condition ($\rho + p_r < 0$) for the values of parameters $r_0 = 1$ and $\rho_0 = 0.0001$

III. CONCLUSION

Existence of wormholes is an important problem in physics both at micro and macro scales. There is no doubt that together with black holes wormholes constitute the most interesting objects in our entire universe. On the one hand collision of ultra-energetic particles may create these objects while at the other extreme they form in galactic systems of cosmic dynamics. Once formed in order to survive wormholes must satisfy certain criteria of stability, otherwise they will decay instantly into stable objects. Besides stability energy conditions are also of prime importance concerning wormholes. This demands negative energy density which is not available in classical physics although there are rooms for it in the quantum domain. Let us add also that a recent trend is to modify the geometry of throats and obtain thin-shell wormholes [33, 34] supported by positive total energy, for this see [35] and references cited therein. However, the minimum requirement of violating null-energy condition (NEC) provides that $\rho + p_r < 0$, without specifying the (-) condition for the energy density. As a matter of fact NEC provides us a jumping board into the realm of wormholes. Stability, on the other hand, admittedly, remains open in our present study.

This work is motivated by Ref. [2], which discusses the possible formation/existence of wormholes in our own galaxy, Milky Way. Their conclusion that wormholes may exist both at the inner and outer parts of our spiral galaxy has been revised by using a different density distribution. Namely, we adapt the Einasto density profile [4, 5] which differs much from the Navarro- Frenk- White (NFW) profile employed in [2, 7]. Our analysis suggests accordingly that at the central region since the NEC is not violated, we do not get wormholes. Yet at the outer regions, the NEC is violated so flare-out condition for wormhole is satisfied and we expect formation of wormholes. This result is not specific to Milky Way alone but is valid for any spiral galaxy once it obeys a mass distribution given by Einasto profile. It is worthwhile therefore to check other mass distributions and see the resulting consequences. There may even be dark matter lurking in our own solar system, which is in the innermost part of the Milky Way [12], and if that's so, may be it supports the existence of wormhole in the solar system.

-
- [1] F. Rahaman, P.K.F. Kuhfittig, S. Ray, N. Islam, Eur. Phys. J. C **74**, 2750 (2014).
 - [2] F. Rahaman, P. Salucci, P.K.F. Kuhfittig, M. Rahaman, Annals of Phys. **350**, (2014) 561-567.
 - [3] P.K.F. Kuhfittig, Eur. Phys. J. C **74**, 2818 (2014).
 - [4] J. Einasto, Trudy Inst. Astrofiz. Alma-Ata **5**, 87 (1965).
 - [5] J. Einasto, U. Haud, Galaxy Astron. Astrophys. **223**, 89 (1989).
 - [6] D. Merritt, A. Graham et al., The Astronomical Journal **132**, 6, 2685 (2006).
 - [7] J.F. Navarro, C.S. Frenk, S.D.M. White, Astrophys. J. **462**, 563 (1996).

- [8] G. Castignani, N. Frusciante, D. Vernieri, P. Salucci, Nat. Sci. **4**, 265 (2012).
- [9] J. Hjorth, L.L.R. Williams, R. Wojtak, M. McLaughlin, **arXiv:1508.02195**.
- [10] A.A. Dutton, A.V. Maccio, MNRAS **441** (4), 3359 (2014).
- [11] I. Siutsou, C.R. Argüelles, R. Ruffini, Astronomy Reports **59**, 7, 656 (2015).
- [12] F. Iocco, M. Pato, G. Bertone, Nature Physics **11**, 245 (2015).
- [13] N. Bernal, S. Palomares-Ruiz JCAP **01**, 006 (2012).
- [14] E. Salvador-Sole, J. Vinas, A. Manrique, S. Serra, MNRAS **423** (3), 2190 (2012) .
- [15] B.K. Dhar and L.L.R. Williams, MNRAS **405** (1), 340 (2010).
- [16] T. Narikawa, K. Yamamoto, JCAP **05**, 016 (2012).
- [17] C.A. Vera-Ciro, A. Helmi, E. Starkenburg, M.A. Breddels, MNRAS **428** (2), 1696 (2013).
- [18] K. Umetsu, A. Zitrin, et al., **arXiv:1507.04385**.
- [19] M.R. Lovell, C.S. Frenk, et al., MNRAS **439** (1), 300 (2014).
- [20] M. Pato, F. Iocco, ApJ. **803**, L3 (2015).
- [21] M. Pato, F. Iocco, G. Bertone, **arXiv:1504.06324**.
- [22] Abramowitz, M. and Stegun, I. A. (Eds.), Handbook of Mathematical Functions with Formulas, Graphs, and Mathematical Tables, 9th printing. New York: Dover, 1972.
- [23] M.S. Morris, K.S. Thorne, Am. J. Phys. **56**, 395 (1988).
- [24] N. Bozorgnia et al, JCAP *1312*, 050 (2013).
- [25] S. Chandrasekhar, Mathematical Theory of Black Holes (Oxford Classic Texts, 1983).
- [26] L.D. Landau and E.M. Lifshitz, The Classical Theory of Fields (Oxford, Pergamon Press, 1975).
- [27] Jeffreys, H. and Jeffreys, B. S. "The Exponential and Related Integrals." §15.09 in Methods of Mathematical Physics, 3rd ed. Cambridge, England: Cambridge University Press, pp. 470-472, 1988.
- [28] F. Rahaman, M. Kalam, A. De Benedictis, A.A. Usmani, S. Ray, MNRAS **27**, 389 (2008).
- [29] K.K. Nandi, A.I. Filippov, F. Rahaman, et al., MNRAS **399**, 2079 (2009).
- [30] F. Nesti, P. Salucci, MNRAS **7**, 16 (2013).
- [31] A.V. Maccio, et al., ApJ Lett. **744**, L9 (2012).
- [32] N.W. Evans, A.A. Williams, MNRAS **443** (1), 791 (2014).
- [33] M. Halilsoy, A. Ovgun, S.H. Mazharimousavi, Eur.Phys.J. C **74**, 2796 (2014).
- [34] A. Ovgun, I. Sakalli, **arXiv:1507.03949**.
- [35] S.H. Mazharimousavi, M. Halilsoy, Eur.Phys.J. C **75** 6, 271 (2015).